COLLISIONAL QUENCHING OF ATOMIC AND MOLECULAR NITROGEN: I. EXPERIMENTAL RESULTS

VON KÁRMÁN GAS DYNAMICS FACILITY
ARNOLD ENGINEERING DEVELOPMENT CENTER
AIR FORCE SYSTEMS COMMAND
ARNOLD AIR FORCE STATION, TENNESSEE 37389

December 1975

Final Report for Period July 1, 1973 to June 30, 1975

Approved for public release; distribution unlimited.

Prepared for

DIRECTORATE OF TECHNOLOGY
ARNOLD ENGINEERING DEVELOPMENT CENTER
ARNOLD AIR FORCE STATION, TENNESSEE 37389

NOTICES

When U. S. Government drawings specifications, or other data are used for any purpose other than a definitely related Government procurement operation, the Government thereby incurs no responsibility nor any obligation whatsoever, and the fact that the Government may have formulated, furnished, or in any way supplied the said drawings, specifications, or other data, is not to be regarded by implication or otherwise, or in any manner licensing the holder or any other person or corporation, or conveying any rights or permission to manufacture, use, or sell any patented invention that may in any way be related thereto.

Qualified users may obtain copies of this report from the Defense Documentation Center.

References to named commercial products in this report are not to be considered in any sense as an endorsement of the product by the United States Air Force or the Government.

This report has been reviewed by the Information Office (OI) and is releasable to the National Technical Information Service (NTIS). At NTIS, it will be available to the general public, including foreign nations.

APPROVAL STATEMENT

This technical report has been reviewed and is approved for publication.

FOR THE COMMANDER

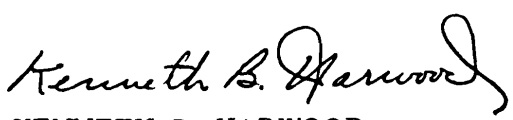

KENNETH B. HARWOOD
Captain, CF
Research & Development
Division
Directorate of Technology

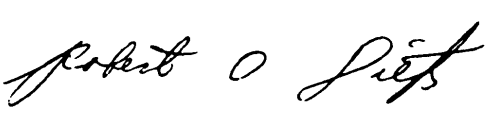

ROBERT O. DIETZ
Director of Technology

REPORT DOCUMENTATION PAGE		READ INSTRUCTIONS BEFORE COMPLETING FORM
1. REPORT NUMBER AEDC-TR-75-151	2. GOVT ACCESSION NO.	3. RECIPIENT'S CATALOG NUMBER
4. TITLE (and Subtitle) COLLISIONAL QUENCHING OF ATOMIC AND MOLECULAR NITROGEN: I. EXPERIMENTAL RESULTS		5. TYPE OF REPORT & PERIOD COVERED Final Report - July 1, 1973 to June 30, 1975 6. PERFORMING ORG. REPORT NUMBER
7. AUTHOR(s) L. L. Price and J. W. L. Lewis, ARO, Inc.		8. CONTRACT OR GRANT NUMBER(s)
9. PERFORMING ORGANIZATION NAME AND ADDRESS Arnold Engineering Development Center (DY) Air Force Systems Command Arnold Air Force Station, Tennessee 37389		10. PROGRAM ELEMENT, PROJECT, TASK AREA & WORK UNIT NUMBERS Program Elements 65802F and 65807F
11. CONTROLLING OFFICE NAME AND ADDRESS Arnold Engineering Development Center(DYFS) Air Force Systems Command Arnold Air Force Station, Tennessee 37389		12. REPORT DATE December 1975 13. NUMBER OF PAGES 36
14. MONITORING AGENCY NAME & ADDRESS(if different from Controlling Office)		15. SECURITY CLASS. (of this report) UNCLASSIFIED 15a. DECLASSIFICATION DOWNGRADING SCHEDULE N/A

16. DISTRIBUTION STATEMENT (of this Report)

Approved for public release; distribution unlimited.

17. DISTRIBUTION STATEMENT (of the abstract entered in Block 20, if different from Report)

18. SUPPLEMENTARY NOTES

Available in DDC

19. KEY WORDS (Continue on reverse side if necessary and identify by block number)

electron beams	fluorescence
nitrogen	electronic state
quenching	intensity

20. ABSTRACT (Continue on reverse side if necessary and identify by block number)

High energy electron beam collisions with N_2 have been used to produce various fluorescent emission systems, the intensities of which were investigated over the approximate pressure range of 0.1 to 2.0 torr at both 300 and 94 K. Specifically, the intensities of the N_2^+ first negative system, the 493.5-nm N line, and the 500.5-nm N^+ line were observed as a function of N_2 pressure, and the results were used to determine the quenching rate constants for these excited electronic states.

DD FORM 1 JAN 73 1473 EDITION OF 1 NOV 65 IS OBSOLETE

PREFACE

The work reported herein was conducted by the Arnold Engineering Development Center (AEDC), Air Force Systems Command (AFSC). The results of the research were obtained by ARO, Inc. (a subsidiary of Sverdrup & Parcel and Associates, Inc.), contract operator of AEDC, AFSC, Arnold Air Force Station, Tennessee, under ARO Project Numbers VF420 and V32S-46A. The authors of this report were L. L. Price and J. W. L. Lewis, ARO, Inc. The manuscript (ARO Control No. ARO-VKF-TR-75-111) was submitted for publication on June 30, 1975.

CONTENTS

ILLUSTRATIONS

Figure | Page

TABLES

1.0 INTRODUCTION

1.1 BACKGROUND

Electron beam diagnostics have provided nonperturbing and spatially resolved measurements of number density, velocity distribution functions, and rotational and vibrational temperatures in gaseous flows of a limited number of species. Extension of the technique is required to include more species, more parameters, and a better understanding of the physical processes underlying the excitation and emission processes. Such a program has been accomplished at AEDC for several years, with many subsequent practical applications.

Nitrogen is the most abundant gas in the atmosphere, is the only constituent in many high enthalpy wind tunnel flows, and has been exploited by the electron beam technique more than any other species. The parameter measured in quenching experiments is a rate constant descriptive of loss of emitted radiation at elevated densities. Specifically, as the density increases, collisions of excited species with nitrogen molecules result in collisional energy transfer from the excited state rather than in the emitted radiation of interest. Consequently, the use of fluorescence diagnostics at high densities involves a correction because of this collisional transfer process.

In the studies reported herein, detailed collisional de-excitation, or quenching, measurements were performed on radiation from the ionized nitrogen molecule, N_2^+; atomic nitrogen, N; and singly ionized atomic nitrogen, N^+; as quenched by molecular nitrogen, N_2. The material presented in the following sections represents the experimental results of this work.

Electron-beam-excited emission from the P and R branches of the (0,0) band of the first negative system of nitrogen, $N_2^+(1-)$, is commonly used for number density and rotational temperature measurements. Experimental evidence has shown that theoretical descriptions of the excitation-emission process have failed to account for density-dependent, R-branch rotational line intensity distributions, and for this reason the measurement of quenching rate constants of resolved R-branch lines was undertaken. In addition, quenching rate constants of the unresolved (0,0) and (1,2) P-branch

bandheads, the (1, 2) fifth R-branch rotational line, $N[2p^2(^3P)4p\ ^2S^o_{1/2} \rightarrow 2p^23s\ ^2P_{3/2}]$ at 4935.03 Å and $N^+[2p(^2P^o)3d\ ^3F^o_4 \rightarrow 2p3p\ ^3D_3]$ at 5005.14 Å were determined.

1.2 EXCITATION-DECAY PROCESSES OF N_2

Molecular nitrogen is directly excited by electron impact to the $N_2^+B^2\Sigma_u^+$ electronic state:

$$N_2X\,^1\Sigma_g^+(v') + e^- \rightarrow N_2^+B^2\Sigma_u^+(v) + 2e^-$$

from which spontaneous radiation occurs by

$$N_2^+B^2\Sigma_u^+(v) \rightarrow N_2^+X^2\Sigma_g^+(v'') + h\nu(1\text{-})(v,v'')$$

The collisional de-excitation process is

$$N_2^+B^2\Sigma_u^+(v) + N_2X\,^1\Sigma_g^+(v') \rightarrow N_2^+(\alpha) + N_2(\beta)$$

in which the final states α and β are unknown.

The excitation process of atomic nitrogen for the $2p^2(^3P)4p\ ^2S^o_{1/2}$ state is

$$N_2X\,^1\Sigma_g^+(v') + e^- \rightarrow N\left[2p^2(^3P)4p\,^2S^o_{1/2}\right] + N(\epsilon) + e^-$$

from which spontaneous radiation occurs by

$$N\left[2p^2(^3P)4p\ ^2S^o_{1/2}\right] \rightarrow N(2p^23s\ ^2P_{3/2}) + h\nu(4935.03\ \text{Å})$$

and quenching is by

$$N\left[2p^2(^3P)4p\ ^2S^o_{1/2}\right] + N_2X\,^1\Sigma_g^+(v') \rightarrow N(\gamma') + N_2(\beta')$$

where ϵ, γ', and β' are unspecified states.

For the nitrogen atomic ion state $N^+[2p(^2P^o)3d\ ^3F_4^o]$, excitation is by

$$N_2X^2\Sigma_g^+(v') + e^- \rightarrow N^+\left[2p(^2P^o)3d\ ^3F_4^o\right] + N(\xi) + 2e^-$$

from which spontaneous radiation occurs by

$$N^+\left[2p(^2P^o)3d\ ^3F_4^o\right] \rightarrow N^+(2p3p\ ^3D_3) + h\nu\ (5005.14\text{Å})$$

and quenching is by

$$N^+\left[2p(^2P^o)3d\ ^3F_4^o\right] + N_2X^1\Sigma_g^+(v') \rightarrow N^+(\delta) + N_2(\beta'')$$

where ξ, δ, and β'' are unspecified states.

For an atomic radiative transition from state i to j, assuming no quenching or cascading from upper states, the number of photons per second emitted from an electron beam of length L is given by

$$S_o = (I/e)\sigma_{gi}\, n_g\, L(A_{ij}/A_i) \tag{1}$$

where L is the observed length of the electron beam of current I, σ_{gi} is the excitation cross section for the ground state level g→i transition, n_g is the ground state number density, A_{ij} is the Einstein spontaneous transition probability for the i to j transition, and A_i is the transition probability of state i. Observation of the beam with a detection system of efficiency $s(\lambda)$ and solid angle ω results in a detector photon rate of

$$S = S_o(\omega/4\pi)s(\lambda) \tag{2}$$

With quenching collisions of rate constant $k_i(cc^{-1}/sec/molecule)$ the detector photon rate becomes

$$S = (\omega/4\pi)\ s(\lambda)(I/e)\sigma_{gi}\, n_g\, L\, A_{ij}\tau_i/(1 + k_i\tau_i n_g) \tag{3}$$

where $\tau_i = A_i^{-1}$ is the radiative lifetime of state i. Defining C, a constant, to be $(\omega/4\pi)s(\lambda)\sigma_{gi}LA_{ij}\tau_i/e$, the radiative intensity, S, can be written as

$$S = C \cdot I \cdot n_g/(1 + k_i\tau_i n_g) \tag{4}$$

or

$$n_g/(S/I) = (1 + k_i\tau_i n_g)/C \tag{5}$$

A plot of $n_g/(S/I)$ versus n_g yields a straight line of slope $k_i\tau_i/C$ and intercept $1/C$; thus, the ratio of slope to intercept gives the value of $k_i\tau_i$. Note that it is the product $k_i\tau_i$ that determines the relative amount of quenching for a fixed value of n_g.

For molecular radiative transitions the Einstein coefficient is replaced by the electronic rotation-vibration transition line strength. When cascading is present the quenching rate constant is obtained as before, since σ_{gi} is merely replaced by the constant $[\sigma_{gi} + \sum_m (A_{mi}/A_m)\sigma_{gm}]$, where the summation is over states m of energy eigenvalues greater than that of state i.

The quenching rate constant for energy level i, k_i, is, of course, the sum of the partial quenching rates k_{ij} connecting states i and j over all states j. The level quenching rate constant is related to the inelastic cross section $\sigma^2_{in}(i)$ by

$$k_i = \sigma^2_{in}(i)(8RT/\pi\tilde{M})^{1/2} \tag{6}$$

where R is the universal gas constant and $\tilde{M}$ is the reduced molecular weight of the collision partners. The static gas temperature is T. Obviously a hard sphere cross section yields a rate constant which varies with the gas temperature as $T^{1/2}$. A second collision model which is of interest to this work is that which represents an ion-neutral collision for which the $X^+ + Y$ charge-induced dipole of specie Y has a significant bearing on the collision mechanics. The elastic rate constant for this process is known to be given by

$$k_e = 2\pi e(\alpha/\mu)^{1/2} \tag{7}$$

where α is the polarizability of the neutral specie and μ is the reduced mass of X^+ and Y. Obviously, the rate constant for such orbiting collisions is temperature independent. One can define a probability of energy transfer for level i using k_e and k_i by

$$P(i) = k_i/k_e \tag{8}$$

where it is assumed that $k_i \ll k_e$. Consequently, using Eqs. (7) and (8),

$$k_i = k_e P(i) \tag{9}$$

and one sees that for collisions of the type $X^+ + Y$ the temperature dependence observed for k_i may be attributed to P(i) alone.

2.0 EXPERIMENTAL APPARATUS

An overall schematic of the experimental system is presented in Fig. 1. This system was essentially the same as that which is more completely described in Ref. 1.

2.1 COLLISION CHAMBER AND GAS FLOW SYSTEM

Electron beam excitation of the gas occurred within a carefully designed flow liner. As shown in Fig. 2, the cylindrical flow liner was contained within the collision chamber, was preceded by a precooling reservoir, and was immediately followed by the pumping system. Water or liquid nitrogen was circulated within the reservoir and liner walls to achieve constant temperatures, and those wall temperatures as monitored by thermocouples showed no significant gradients. A fully developed laminar Poiseuille flow at the electron beam excitation position existed for all flow conditions, enabling estimates of flow velocity gradients to be made. Additionally, the thermal boundary layer was fully developed before it reached the electron beam excitation region. Any radial gradients in gas temperature are then due to frictional heating, and for this Poiseuille flow case the centerline temperature, T_{max}, for a subsonic flow of centerline Mach number, M, is given by

$$(T_{max} - T_o)/T_{max} = 1/4[Pr(\gamma - 1)M^2]$$

where T_o is the wall temperature; the Prandtl number, Pr, is approximately 0.7; and $\gamma = 1.4$ is the specific heat ratio of nitrogen. For the measurements reported herein, the largest difference between T_{max} and T_o occurred with the $T_o = 77$ K, $P_\infty = 0.10$ torr condition in which, according to the above equation, T_{max} was about two percent greater than T_o.

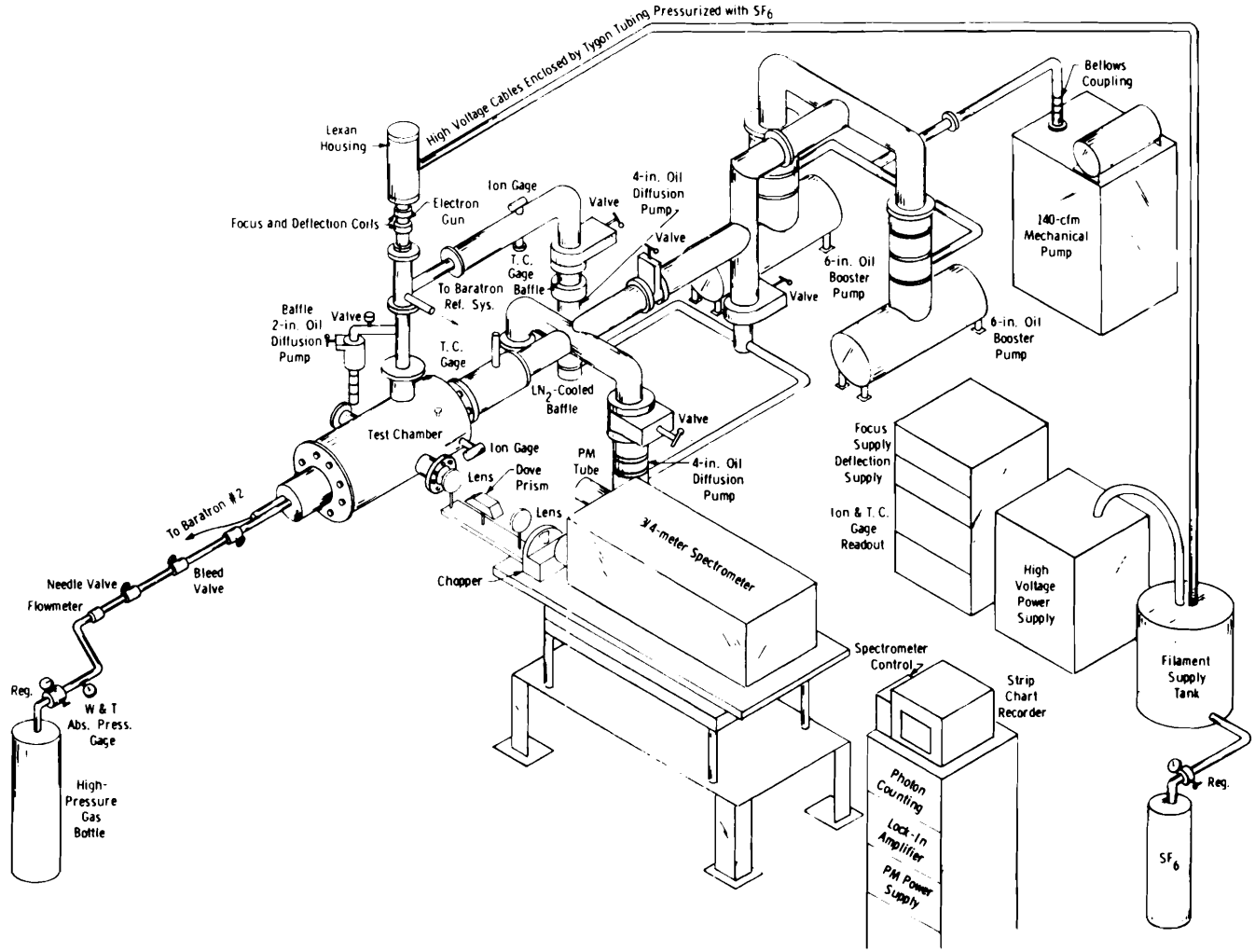

Figure 1. Experimental system.

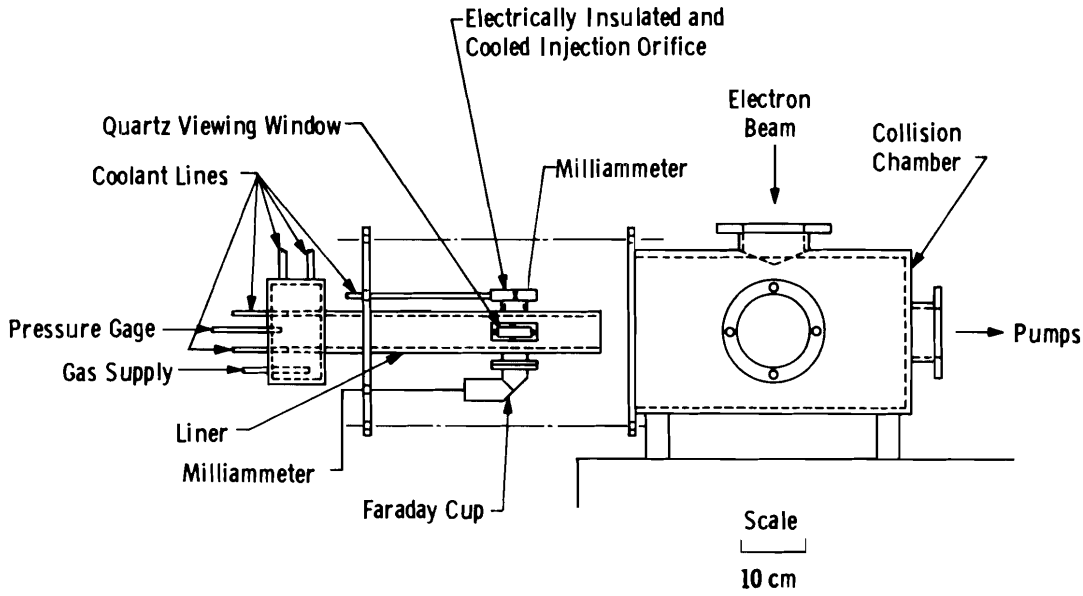

Figure 2. Collision chamber and liner.

The chamber and gas inlet lines were evacuated to a pressure of less than 10^{-5} torr as measured by an ionization gage and then purged with the prepurified nitrogen gas twice before measurements began. Chamber pressures were then measured with an MKS Baratron®

2.2 ELECTRON BEAM SOURCE

Modified television-type electron guns having oxide-coated cathodes provided electrons at 40 keV and up to 1 mA in the observation volume. The cathode emission current was approximately two times the beam current. Magnetic deflection and focusing coils near the gun directed electrons downward through a 1.25-m-long drift tube and two separated 40-mm-diam orifices, which defined the two-stage differential pumping system, before entering the larger collision chamber entrance orifice. Pressures in the gun section remained below 10^{-5} torr for chamber pressures up to two torr. A copper, water-cooled Faraday cup collected the beam current. To suppress the emission of secondary electrons, the cup was coated with colloidal graphite. Also, the L-shaped cup contained a 45-deg deflection plate as the beam target, causing most of the secondary emission from the impinging beam to be absorbed in succeeding cup-wall collisions, thereby minimizing backscattered emission in the observation volume. The high voltage cables of the gun were contained within Tygon® tubing and pressurized with SF_6 gas to prevent arcing and corona discharges.

2.3 OPTICS AND DATA REGISTRATION SYSTEM

The electron beam width at the point of observation increased with increasing chamber pressure. To ensure that no emitted light escaped the detection system as the width varied, a Dove prism was employed to rotate the electron beam image 90 deg so that the electron beam diameter was focused along the slit height. The collecting optics are shown in Fig. 3. The best beam image was obtained with parallel light passing through the Dove prism. To match the dimensions of the Dove prism, the glass 24.8-cm-focal-length collector lens was apertured to a diameter of 2.5 cm, and the achromatic, 21.9-cm-focal-length focusing lens matched the f-number of the spectrometer. The resultant lateral magnification was 0.90. Initial alignment was performed without the Dove prism to ensure a final linear light path.

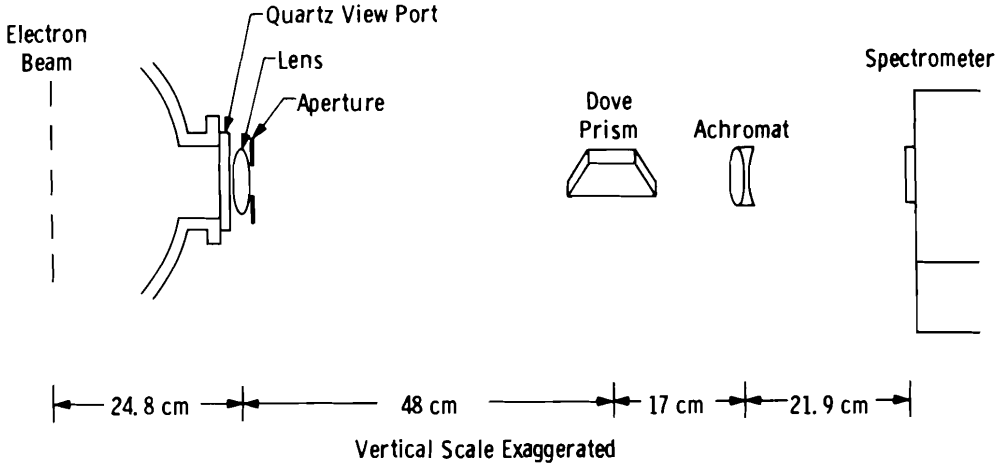

Figure 3. Optical arrangement.

The 0.75-m Spex scanning spectrometer with 1180-groove/mm grating blazed at 5000Å is of Czerny-Turner design. Since the entrance slit height was 22 mm and the magnification 0.9, the slit image upon the chamber observation point covered a horizontal width of 25 mm. Slit widths from 27 to 400 μm were used, the most narrow providing a resolution of 0.3 Å and the widest, a spectral halfwidth of 4.4 Å. Scan rates were from 1.4 to 3.2 Å/min.

The detector was an RCA 7265 photomultiplier tube, which has an S-20 spectral response peaked near 4200 Å. The dark current was significantly lowered by cooling the tube to -20°C with cool nitrogen gas. High voltage was provided by a Kepco model ABC 2500,

regulated d-c power supply. Generally, -2,000 v were provided for the photomultiplier tube, but at several high light levels with wide slits, reductions to as low as -1,210 v were necessary.

Two data registration systems were used and are outlined in Fig. 4. The unresolved $N_2^+(1-)(0,0)$ P-branch measurements utilized a PAR model HR-8 lock-in amplifier for signal processing. Light was chopped at 667 Hz by means of a PAR model 125 chopper located next to the entrance slit. A reference signal at the same frequency was supplied to the amplifier by the chopper. The signal output voltage was recorded by hand. All other measurements utilized the following ORTEC photon counting electronics: Model 454 Timing Filter Amplifier, Model 436 100-MHz Discriminator, Model 441 Ratemeter, and Model 715 Dual Counter/Timer. A 51-Ω photomultiplier output load resistor and maximum amplification were used. For signal recording, a Honeywell Electronik 19 strip-chart recorder registered the analog output of the ratemeter. For fixed wavelength operation, the output was recorded for about 20 sec at constant current for each pressure.

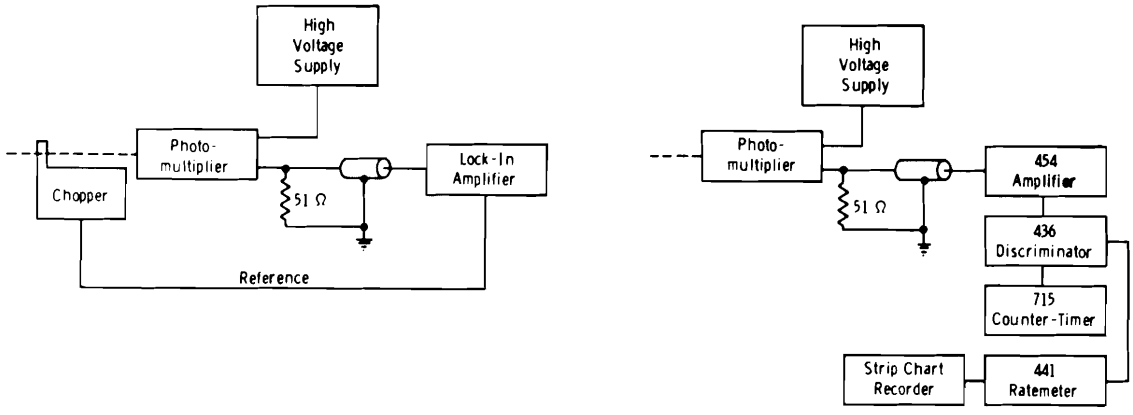

Figure 4. Data registration systems.

3.0 RESULTS

3.1 $N_2^+(1-)(0,0)$ P-BRANCH HEAD

The spectrometer slits were set at 400-μm width and 20-mm height to obtain a halfwidth of 4.4 Å, resulting in an unresolved spectrum and high detection sensitivity. The wavelength was adjusted until the maximum signal was obtained for the room temperature gas case. Previous unpublished measurements at AEDC of this P-branch

head have always shown proportionality between intensity, S, and beam current, I, and between intensity and number density, n_{N_2}, up to the quenching regime.

A typical plot of the current-normalized signal versus N_2 number density is shown in Fig. 5 for 295 K. Background intensity corrections were very small at all densities. The initial data were plotted in terms of pressure, P, instead of number density. Data points of the j^{th} determination that formed the straight line slope of P/(S/I) versus P were then input to a computer program that calculated the least-squares slope, resultant intercept, quenching rate constant k(j), and standard deviation $\sigma(j)$ of the data to the least-squares fit. Figure 6 is the final quenching plot of the data of Fig. 5 including the computer-calculated least-squares slope.

The results are tabulated in Table 1 along with those of the other species and transitions measured. To obtain k from the measured value of $k\tau$, a level lifetime of 6.58×10^{-8} sec was used (Ref. 2). No current dependence of k was noted. The mean value $\bar{k}$ of all measurements and its 2-σ value, which represents the approximate 95-percent confidence level value, are given. These were used in lieu of the weighted mean value k_w and uncertainty σ_w of J individual determinations given by

$$k_w = \sum_{j=1}^{J} \left[k(j)/\sigma^2(j)\right] \Big/ \sum_{j=1}^{J} \left[1/\sigma^2(j)\right]$$

and

$$1/\sigma_w^2 = \sum_{j=1}^{J} \left[1/\sigma^2(j)\right]$$

since it was found that $\sigma > \sigma_w$ in all cases, that is, the precision of each individual measurement exceeded the accuracy. In this case $k_w\tau \pm 2\sigma_w = 1.85 \pm 0.03$ cc, so that $\sigma \cong 10\sigma_w$. In the case of only one or two determinations, estimated standard deviations are given.

The density at which quenching was first observed on a quenching curve was considered as the observed onset density, n_{on}, and the product of $\bar{k}\tau$ and n_{on} was expected to result in a fraction of about 0.1. The calculated onset density was defined as that density at which the emission was reduced by 10 percent, relative to its nonquenched value, and is equal to $0.111/\bar{k}\tau$. These values are listed in Table 2. The observed onset densities are too high, illustrating the care that is needed for diagnostic measurements when $k\tau$ is not known.

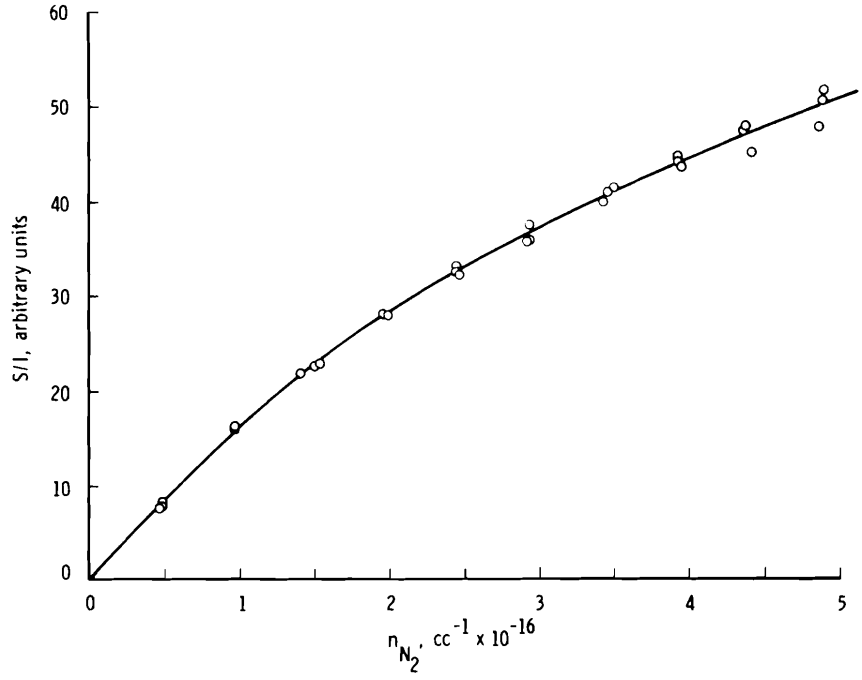

Figure 5. Density variation of N_2^+(1-)(0,0) P-branch intensity at 295 K.

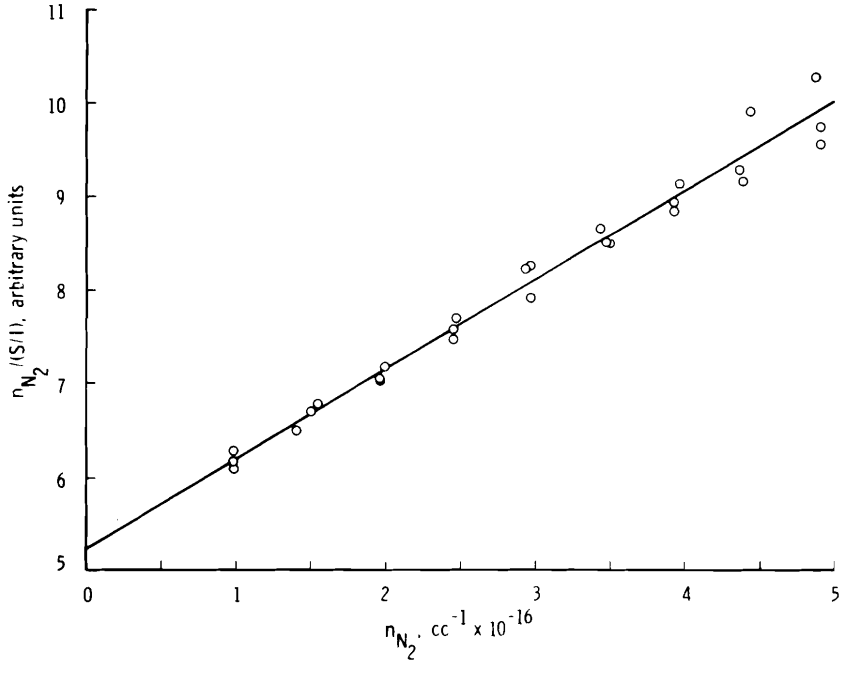

Figure 6. Quenching plot for N_2^+(1-)(0,0) P branch at 295 K.

Table 1. Experimental Results

Species	Transition	Wavelength, angstroms	Temperature, Kelvin	Current, mA	Number of Measurements	$\bar{k}_T \pm 2\sigma$, cc/molecule x 10^{17}	$\bar{k} \pm 2\sigma$, cc/sec/molecule x 10^{10}	$\sigma_{in} \pm 2\sigma$, $Å^2$
N_2^+	(1-)(0,0)P	3914	295 94	0.4-1.2 0.3-1.4	7 3	1.9 ± 0.3 3.5 ± 0.4	2.9 ± 0.4 5.4 ± 0.6	44 ± 6 142 ± 16
N_2^+	(1-)(0,0)R5	3907.8	300 94 300 94	0.8-1.1 0.9-1.2 0.4 0.4	6 4 2 2	1.8 ± 0.2 3.4 ± 0.5 2.1 ± 0.3 4.3 ± 0.8	2.7 ± 0.3 5.1 ± 0.8 3.2 ± 0.4 6.5 ± 1.2	40 ± 4 135 ± 21 47 ± 6 170 ± 30
N_2^+	(1-)(0,0)R	3892-3911 3902-3911	300 94	0.8-1.2 0.8-1.2	3 (18 lines) 1 (11 lines)	1.4 ± 0.2 2.5 ± 0.4	2.2 ± 0.3 3.8 ± 0.6	32 ± 4 102 ± 16
N_2^+	(1-)(1,2)P	4236	294	0.9-1.1	1	2.1 ± 0.3	3.3 ± 0.4	50 ± 6
N_2^+	(1-)(1,2)R5	4227	293	0.8-1.0	2	1.9 ± 0.3	3.0 ± 0.4	45 ± 6
N	$2p^2(^3P)4p\ ^2S^o_{\frac{1}{2}}$ $\rightarrow 2p^2 3s\ ^2P_{3/2}$	4935	292 94	0.9-1.1 1.0-1.1	2 1	16 ± 2 22 ± 4	3.8 ± 0.4 5.1 ± 0.9	47 ± 5 110 ± 19
N^+	$2p(^2P^o)3d\ ^3F^o_4$ $\rightarrow 2p3p\ ^3D_3$	5005	300 94	0.9-1.0 1.0	2 1	4.2 ± 0.5 6.6 ± 1.0	51 ± 6 80 ±12	620 ± 75 1750 ±270

LEGEND: P P Branch
R R Branch
R5 Fifth Rotational Line of R Branch

Table 2. Calculated and Observed Onset Densities

Species	Transition	Temperature, Kelvin	Quenching Onset Density, n_{on}, molecules/cc	$\bar{k}_\tau n_{on}$	Calculated Onset Density, $0.111/\bar{k}_\tau$, molecules/cc	Second Quenching Onset Density, molecules/cc	Second Quenching, k_τ, cc/molecule x 10^{17}
N_2^+	(1-)(0,0)P	295 94	1.1×10^{16} 1.1×10^{16}	0.21 0.38	5.8×10^{15} 3.2×10^{15}	$> 6 \times 10^{16}$ 7×10^{16}	- 1.6
N_2^+	(1-)(0,0)R5	300 94	1.0×10^{16} 5.7×10^{15}	0.18 0.19	6.2×10^{15} 3.3×10^{15}	$> 7 \times 10^{16}$ $> 5 \times 10^{16}$	- -
N_2^+	(1-)(0,0)R	300 94	1.1×10^{16} 6.2×10^{15}	0.15 0.16	7.9×10^{15} 4.4×10^{15}	$> 6 \times 10^{16}$ 4×10^{16}	- > low dens. k_τ
N_2^+	(1-)(1,2)P	294	1.1×10^{16}	0.23	5.3×10^{15}	$> 5 \times 10^{16}$	-
N_2^+	(1-)(1,2)R5	293	1.5×10^{16}	0.29	5.8×10^{15}	$> 5 \times 10^{16}$	-
N	$2p^2(^3P)4p\ ^2S^o_{\frac{1}{2}}$ $\rightarrow 2p^2 3s\ ^2P_{3/2}$	292 94	3.1×10^{15} 3.8×10^{15}	0.50 0.83	6.9×10^{14} 5.1×10^{14}	2.2×10^{16} 2.4×10^{16}	5.6 6.2
N^+	$2p(^2P^o)3d\ ^3F^o_4$ $\rightarrow 2p3p\ ^3D_3$	300 94	7.6×10^{15} 6.8×10^{15}	0.32 0.44	2.6×10^{15} 1.7×10^{15}	$> 5 \times 10^{16}$ $> 4 \times 10^{16}$	- -

LEGEND:
- P — P Branch
- R — R Branch
- R5 — Fifth Rotational Line of R Branch

System alterations during measurements reported herein were followed by room-temperature P-branch quenching measurements to ensure repeatability.

Before beginning the cold-chamber P-branch measurements, resolved $N_2^+(1-)(0,0)$ R-branch scans were made to determine rotational temperatures, T_R, at the observation point. The distributions of electron-beam-excited, rotational line intensities are indicative of the ambient gas temperature. Slit widths of 30 μm were employed, and the spectrum was recorded on a strip-chart recorder as driven by the lock-in amplifier. Although a thermocouple attached to the inside of the liquid-nitrogen (LN_2)-cooled liner indicated less than 88 K, the results as shown in Fig. 7 reveal that for the typical range of reservoir pressures used, 0 to 0.4 torr, the temperature at the point of observation was approximately 94 K.

Since the band shape is a function of temperature, the spectrometer wavelength was changed about 1 Å to obtain the maximum signal at 94 K. Representative data and the final corresponding quenching plot are shown in Figs. 8 and 9. The value obtained at low beam current was only six percent higher than the average of the high current values. A second quenching process at elevated densities is evident in Fig. 9. Its onset density and $k\tau$ value, calculated using a temperature of 120 K, are listed in Table 2. For radiation in which no second quenching was observed, the highest density at which data were taken is listed.

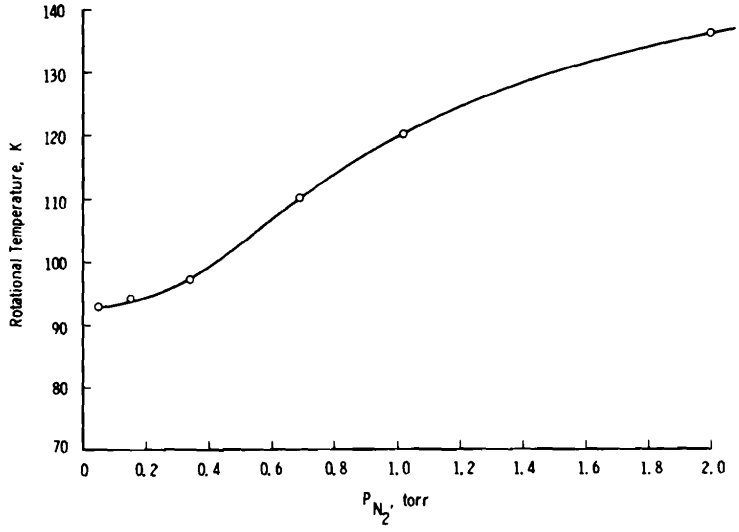

Figure 7. Pressure variation of N_2 rotational temperature for LN_2-cooled chamber.

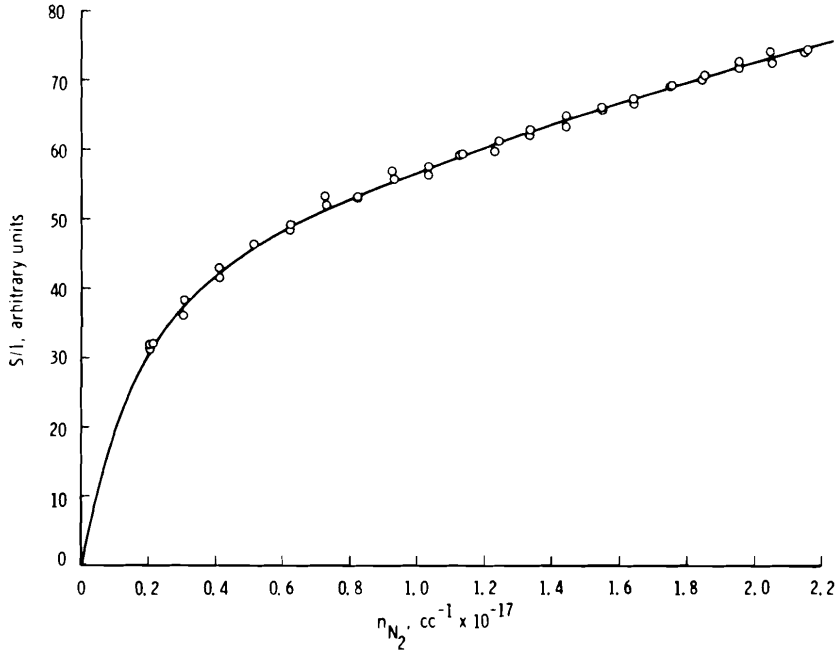

Figure 8. Density variation of N_2^+(1-)(0,0) P-branch intensity at 94 K.

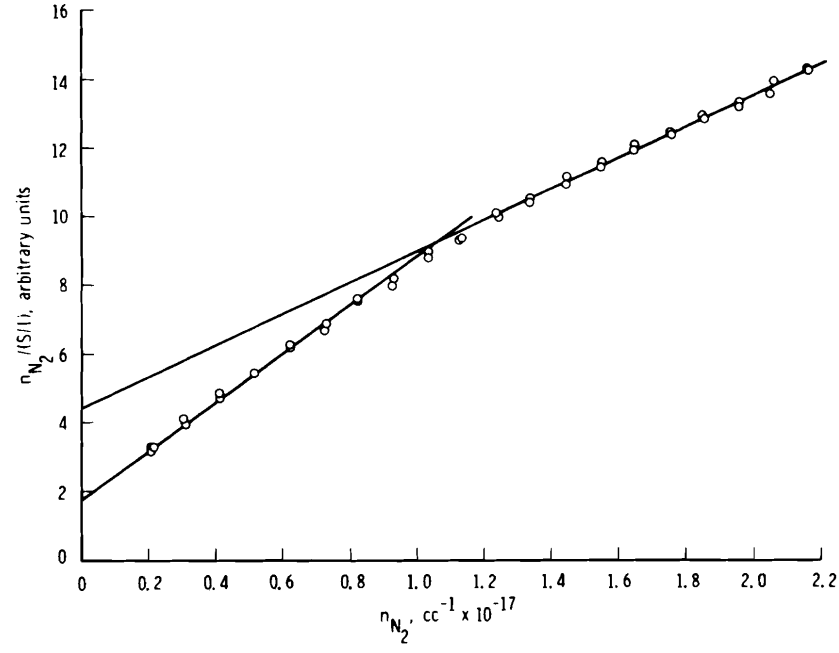

Figure 9. Quenching plot for N_2^+(1-)(0,0) P branch at 94 K.

3.2 $N_2^+(1-)(0,0)$ R-BRANCH ROTATIONAL LINES

Resolved R-branch rotational spectra were obtained with the use of 30-μm slit widths and slow scan rates of about 3 Å/min. The P-branch rotational spectrum was not resolved. The collector current and chamber pressure for each rotational line in each scan were hand-recorded. Beam currents ranged from 0.8 to 1.1 mA. One scan is shown in Fig. 10. Data from one scan set at 300 K for the fifth rotational line is shown in Figs. 11 and 12. The results for 18 lines at 300 K are presented in Fig. 13, in which the error bars represent one standard deviation about the mean value. The lifetime value of $\tau = 6.58 \times 10^{-8}$ sec was used for each line.

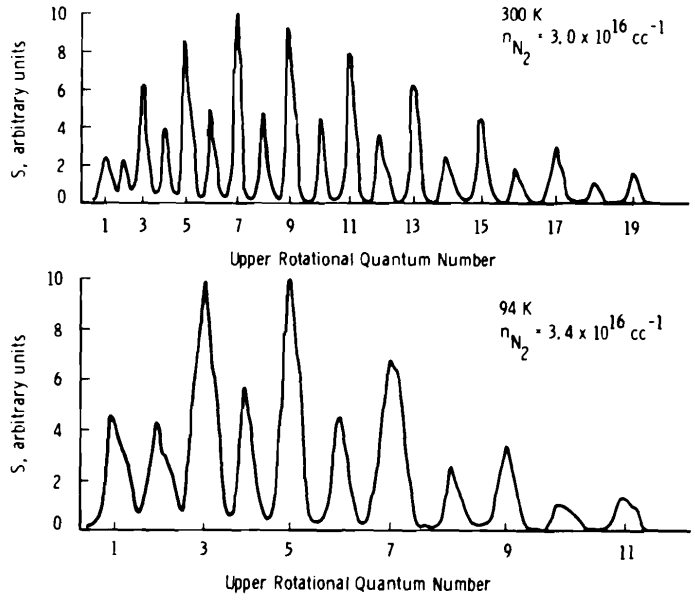

Figure 10. $N_2^+(1-)(0,0)$ R-branch scans at 300 and 94 K.

Only one scan set at 94 K was obtained, and one scan is shown in Fig. 10. Beam currents were from 0.9 to 1.2 mA. According to Fig. 7, the temperature variation over the pressure range used was less than five percent. Final quenching plots suggested a second quenching process at number densities greater than approximately 4×10^{16} cc^{-1}, which is more pronounced for lines from lesser populated rotational states. This is illustrated by the final quenching plot for the seventh rotational line as shown in Fig. 14. Restricting the data to number densities less than 4×10^{16} cc^{-1}, the results in Fig. 15 were obtained for the first eleven rotational lines. The precision of the data is shown by the 1-σ values in Fig. 15.

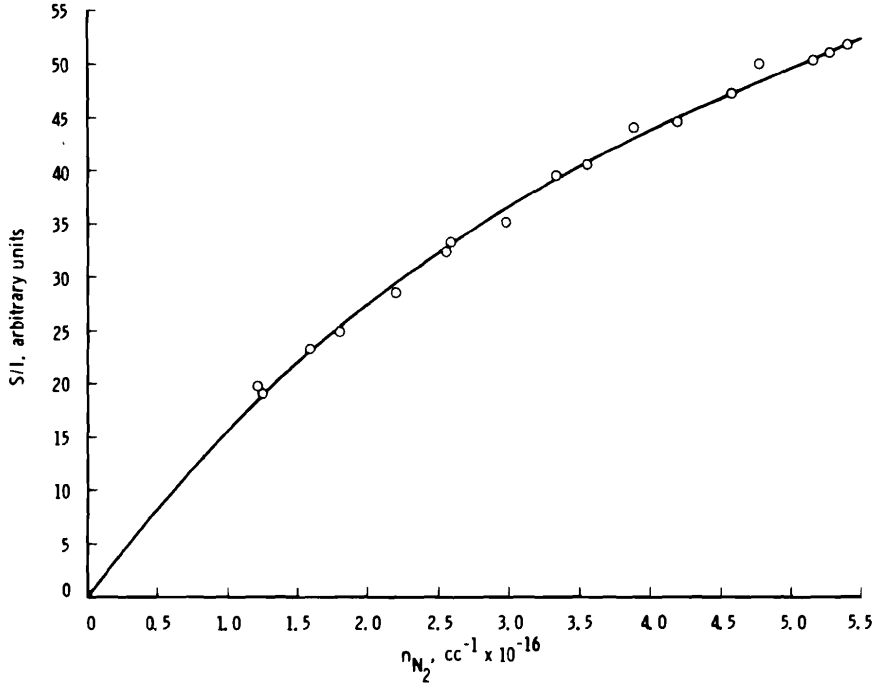

Figure 11. Density variation of $N_2^+(1\text{-})(0,0)$ fifth R-branch rotational line intensity at 300 K.

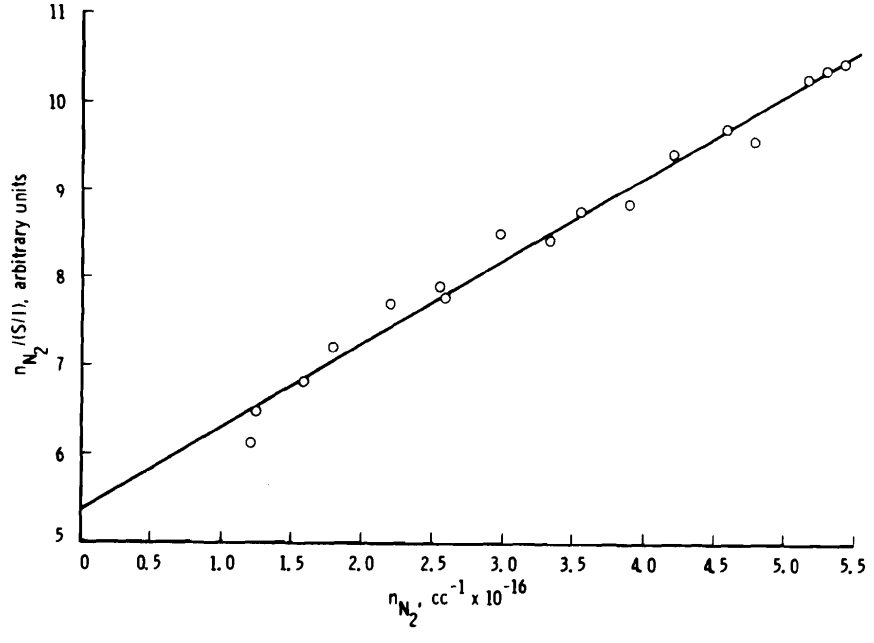

Figure 12. Quenching plot for $N_2^+(1\text{-})(0,0)$ fifth R-branch rotational line at 300 K.

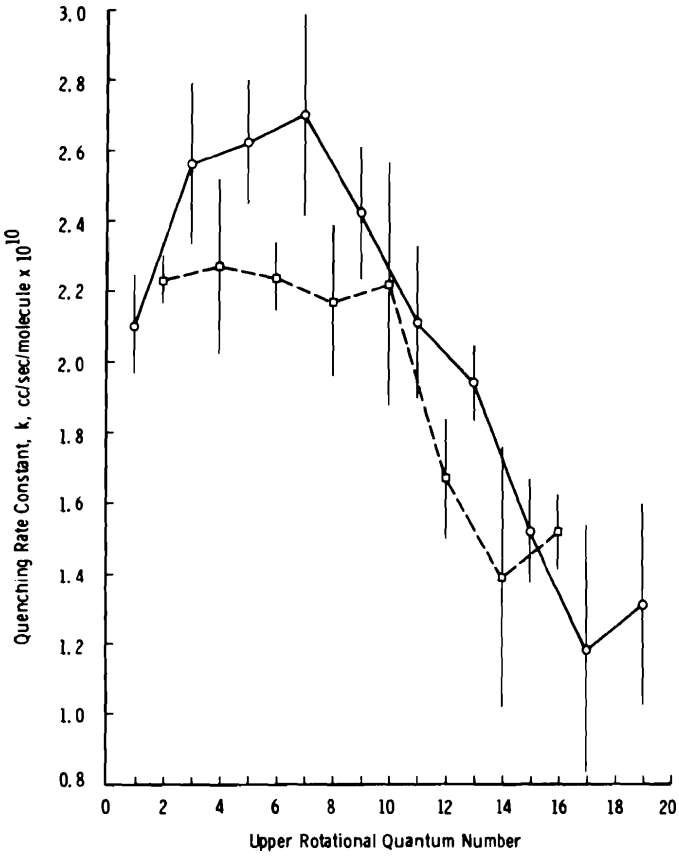

Figure 13. Quenching rate constants for $N_2^+(1\text{-})(0,0)$ R-branch rotational lines at 300 K and N_2 number densities less than 6 x 10^{16} cc^{-1}.

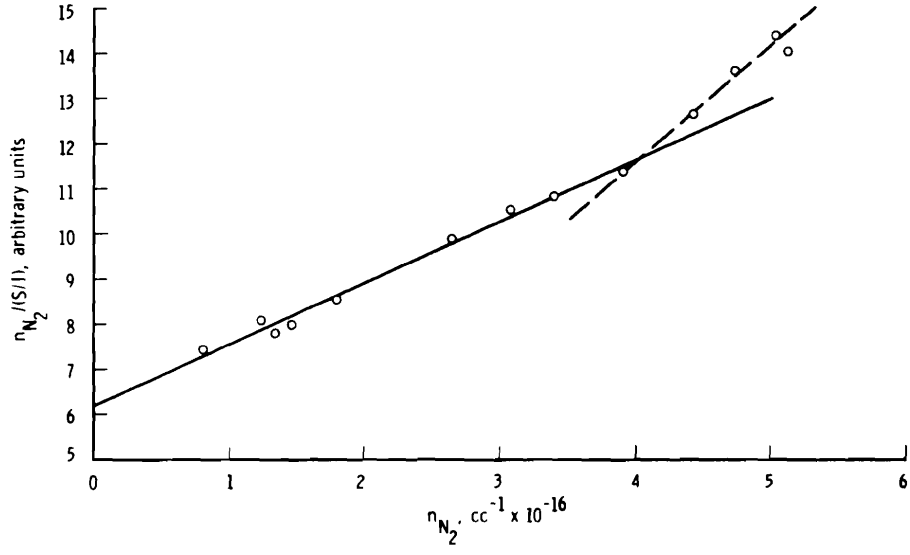

Figure 14. Quenching plot for $N_2^+(1\text{-})(0,0)$ seventh R-branch rotational line at 94 K.

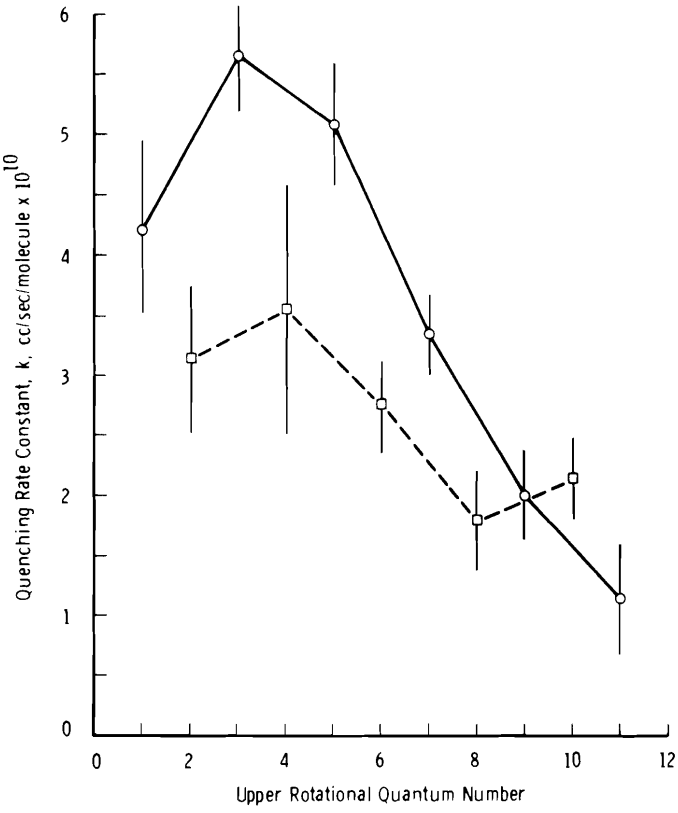

Figure 15. Quenching rate constants for $N_2^+(1-)(0,0)$ R-branch rotational lines at 94 K and N_2 number densities less than 4 x 10^{16} cc^{-1}.

3.3 $N_2^+(1-)(0,0)$ FIFTH R-BRANCH ROTATIONAL LINE

Slit widths were increased to 35 μm to obtain a higher bandpass while retaining sufficient resolution. Data at 300 K verified the behavior of the fifth rotational line as obtained during the R-branch scans and as presented in Figs. 11 and 12. At densities less than 5 x 10^{15} cc^{-1}, however, it appeared that the signal level was less than expected. Figure 16 illustrates this nonlinear response at 1 mA, and the response at 0.4 mA was the same. Detailed measurements at 1 mA in this low density region are shown in Fig. 17.

Experimental quenching rate constants for the fifth rotational line at 300 K, listed in Table 1, appeared to be current dependent and are presented as such. Subsequent measurements of the line

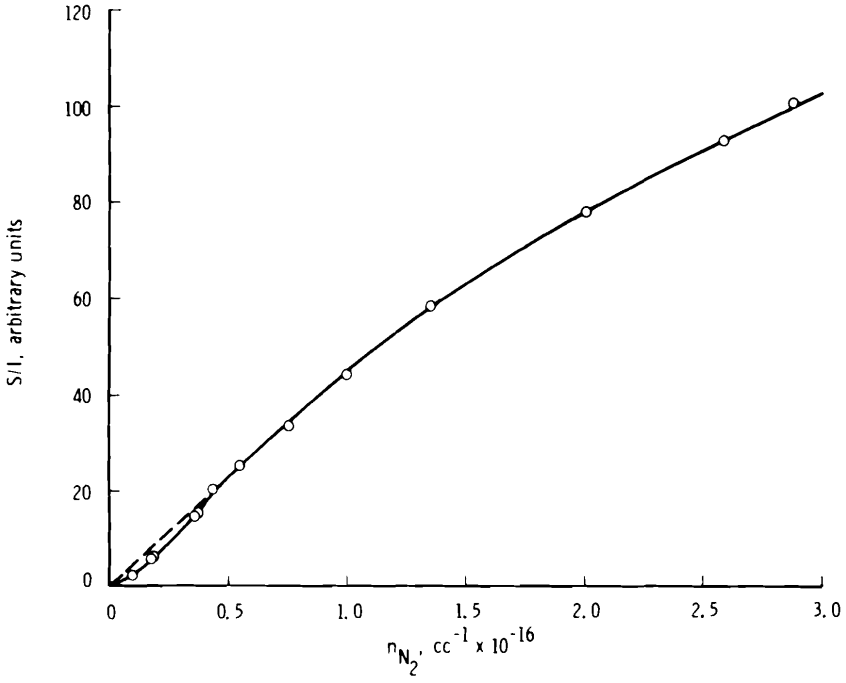

Figure 16. Density variation of $N_2^+(1-)(0,0)$ fifth R-branch rotational line intensity at 300 K.

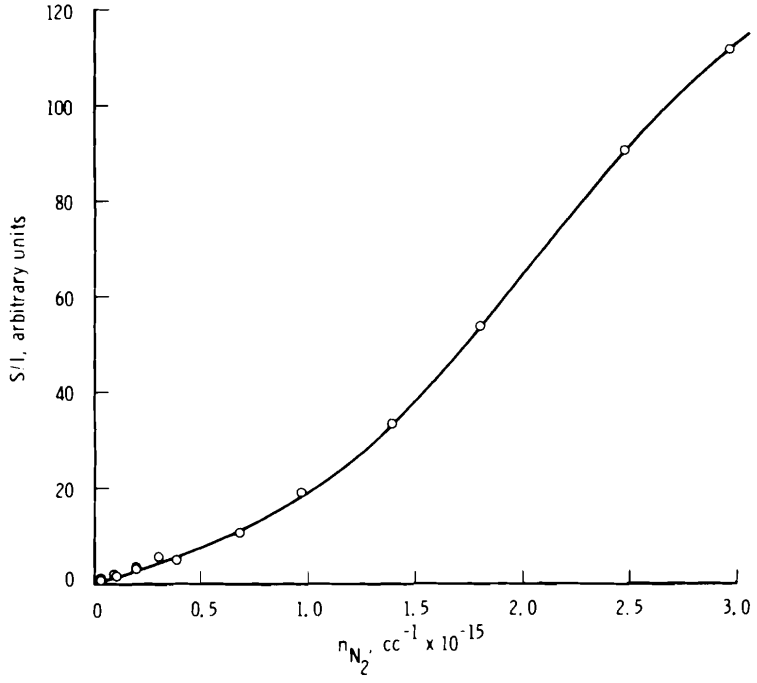

Figure 17. Low density variation of $N_2^+(1-)(0,0)$ fifth R-branch rotational line intensity at 300 K.

intensity as a function of beam current were made at 300 and 94 K and several densities. Figure 18 shows the resultant intensity-current relationship for a nitrogen number density of 1.2×10^{16} cc^{-1} at 300 K, and departure from an extrapolated linear line through the origin below currents of 250 μA was observed. The same response occurred for comparable densities at 94 K. At three times this density, however, the intensity-current relationship at both temperatures changed to that shown in Fig. 19. In these cases the extrapolated linear lines do not go through the origin.

A representative quenching plot at 94 K is presented in Fig. 20. The current-dependent results are listed in Table 1. No evidence was found for a second quenching process below 5×10^{16} cc^{-1}, although a slight effect was observed in the R-branch scan result. Fifth rotational line quenching rate constants determined near 1 mA for 300 and 94 K nitrogen agree well with those determined from the R-branch scans.

3.4 $N_2^+(1^-)(0,0)$ R BRANCH

Quenching rate constants for the unresolved R branch were determined by summing the individual rotational line intensities at each density, $\sum_{\ell}(S_\ell/I_\ell)$. One quenching plot at 300 K and the plot at 94 K are presented in Figs. 21 and 22, respectively, and the results listed in Tables 1 and 2. The evidence for a second quenching process at densities greater than 4×10^{16} cc^{-1} does not appear as strongly in Fig. 22 as it does in quenching plots of lesser populated rotational lines. The sum of intensities of the third and fifth rotational lines at 94 K, which show little or no second quenching, comprise about one-third of the R-branch total intensity and thus have a moderating effect on the visibility of the second quenching.

3.5 $N_2^+(1^-)(1,2)$ P-BRANCH HEAD AND FIFTH R-BRANCH ROTATIONAL LINE

Slit widths of 400 μm duplicated the 4.4-Å halfwidth pass of the (0,0) P-branch head for the (1,2) P-branch head measurement. The (1,2) fifth R-branch line employed 70-μm slit widths. Background signals for both features were determined at the unobstructed wavelength adjacent to the (1,2) P-branch bandhead. Figures 23 and 24 are quenching plots for the two (1,2) band features at room temperature. The experimental results are listed in Table 1. A lifetime for the v = 1 level of $\tau = 6.50 \times 10^{-8}$ sec (Ref. 2) was used.

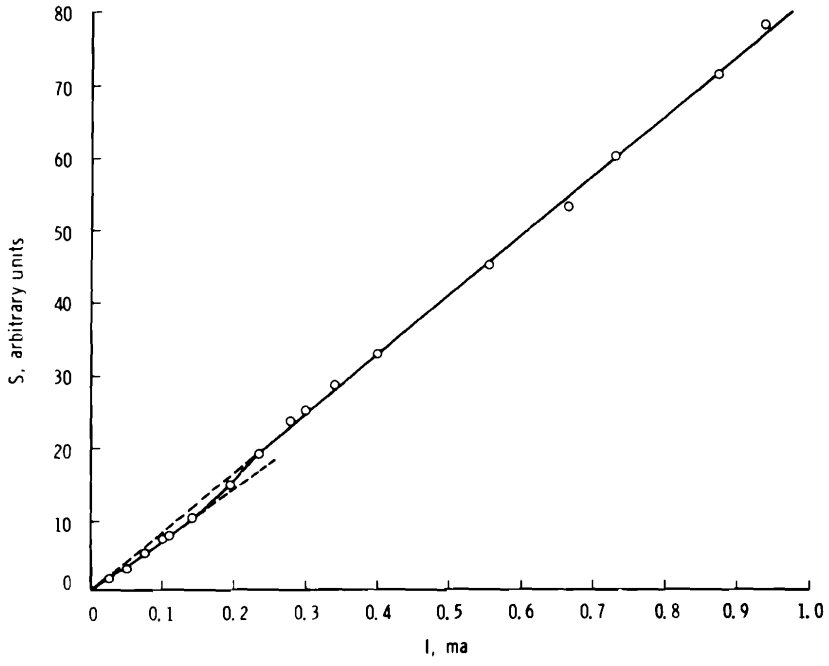

Figure 18. Electron beam current variation of $N_2^+(1\text{-})(0,0)$ fifth R-branch rotational line intensity at 300 K for N_2 number density of 1.2×10^{16} cc^{-1}.

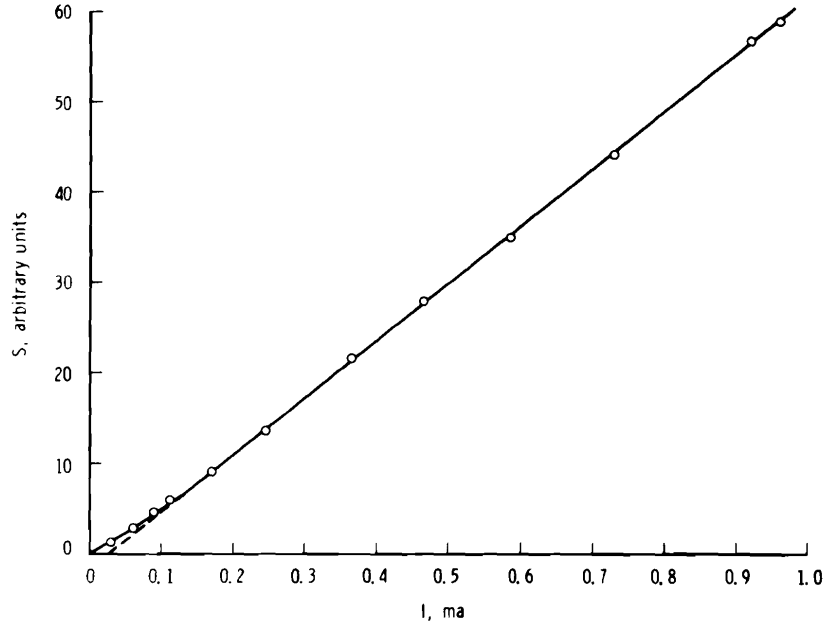

Figure 19. Electron beam current variation of $N_2^+(1\text{-})(0,0)$ fifth R-branch rotational line intensity at 94 K for N_2 number density of 3.7×10^{16} cc^{-1}.

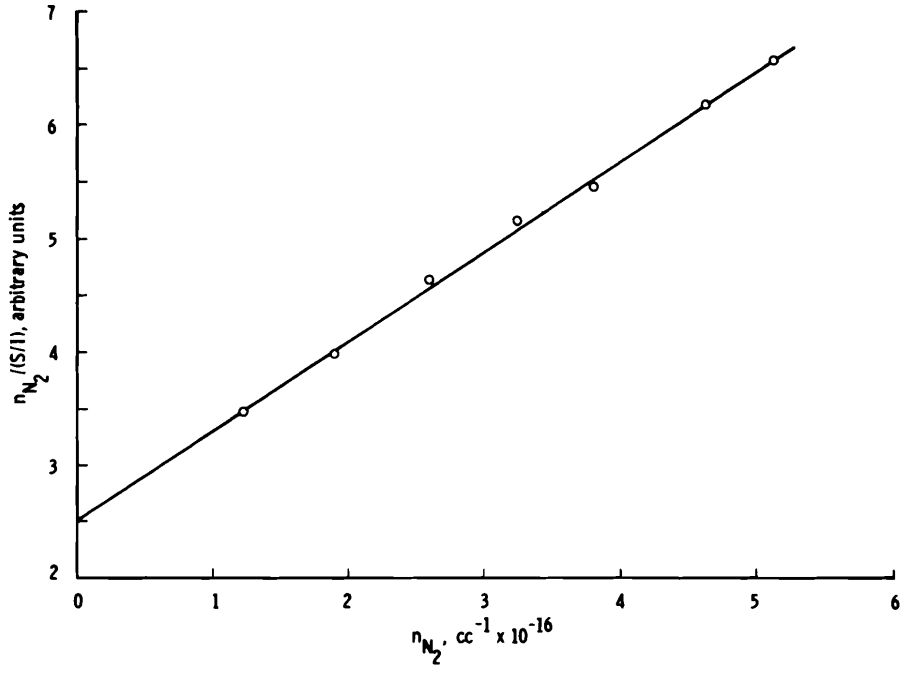

Figure 20. Quenching plot for $N_2^+(1\text{-})(0,0)$ fifth R-branch rotational line at 94 K.

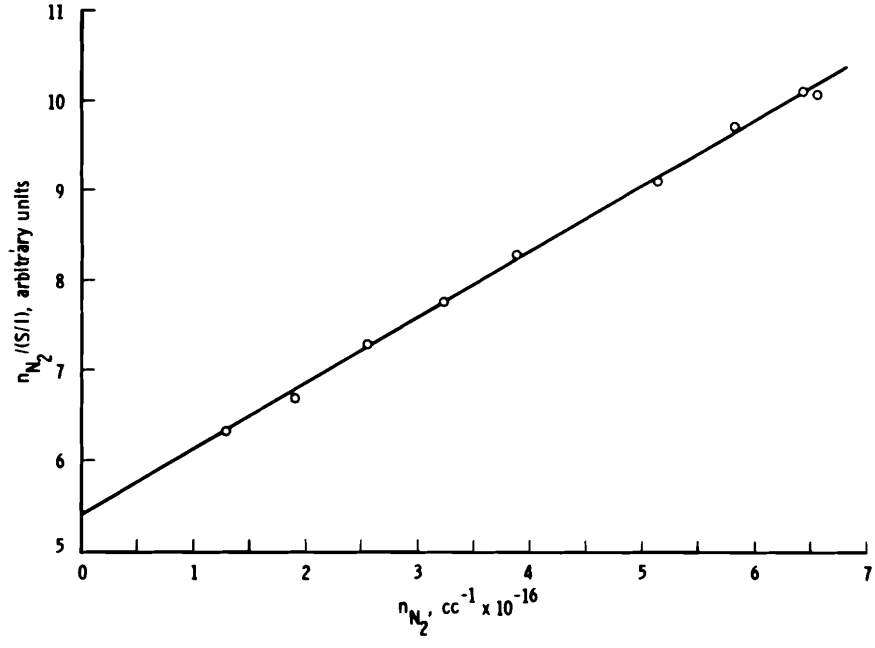

Figure 21. Quenching plot for $N_2^+(1\text{-})(0,0)$ R branch at 300 K.

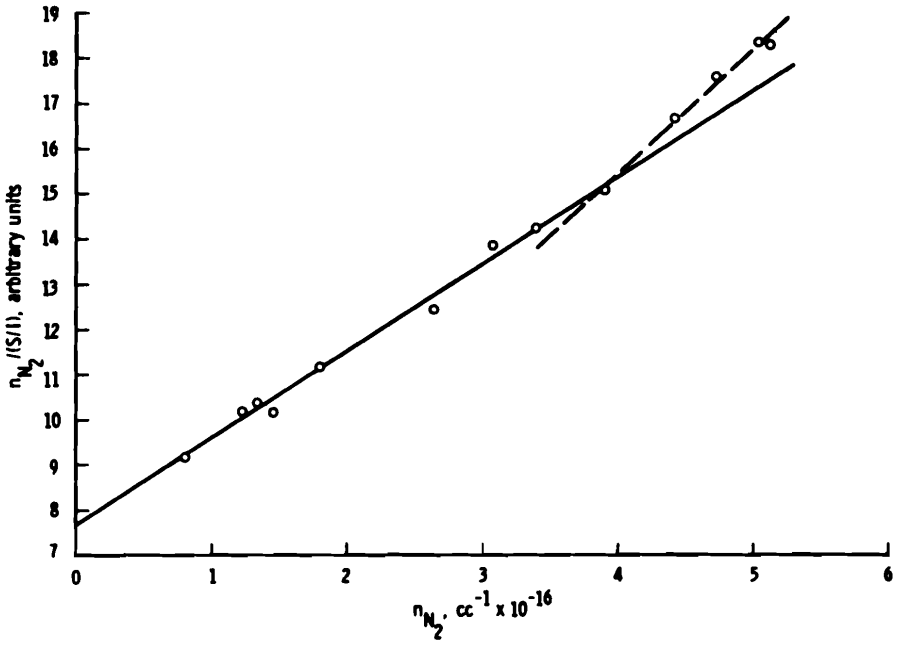

Figure 22. Quenching plot for $N_2^+(1\text{-})(0,0)$ R branch at 94 K.

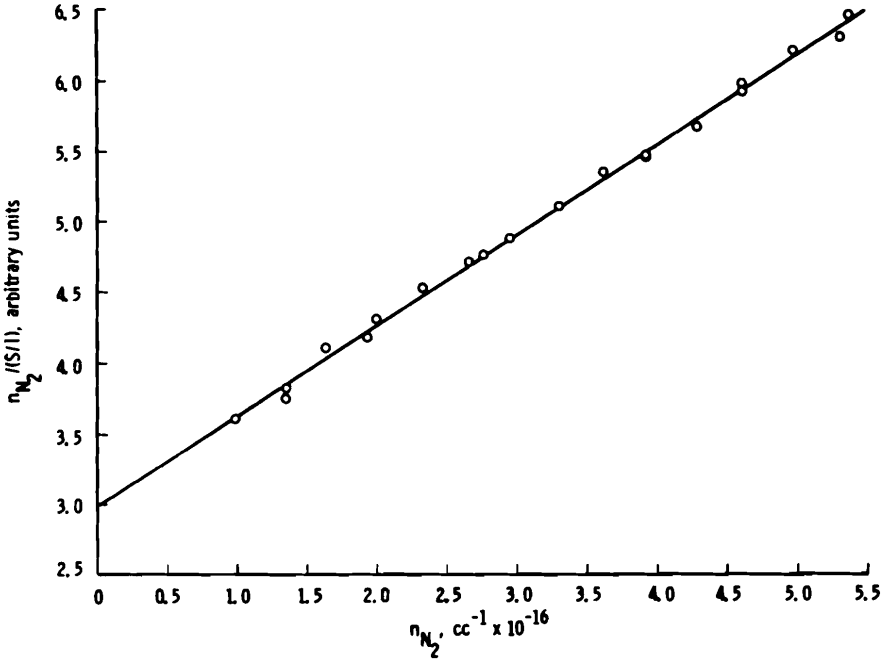

Figure 23. Quenching plot for $N_2^+(1\text{-})(1,2)$ P branch at 294 K.

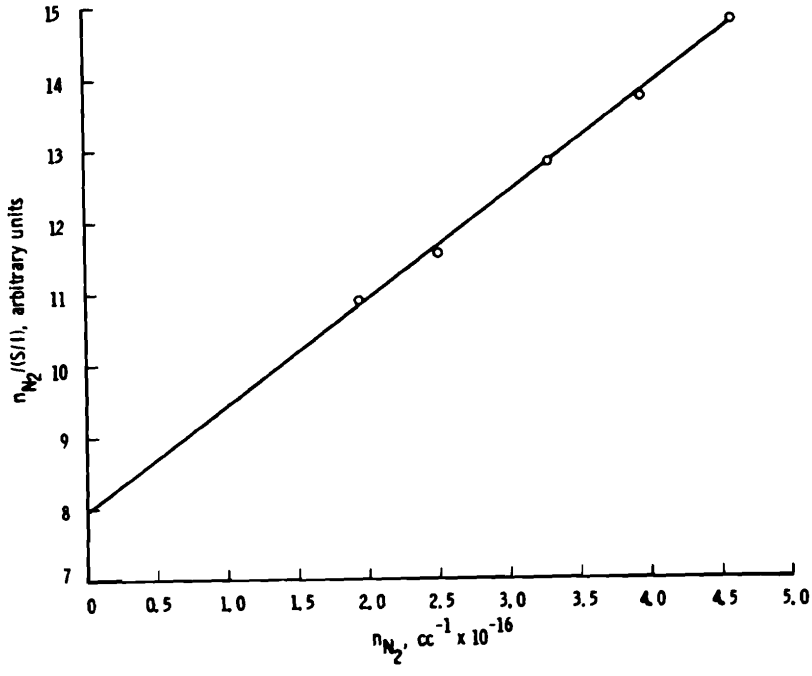

Figure 24. Quenching plot for $N_2^+(1-)(1,2)$ fifth R-branch rotational line at 293 K.

3.6 $N[2p^2(^3P)4p\ ^2S^\circ_{1/2} \rightarrow 2p^2 3s\ ^2P_{3/2}]$

Preliminary spectral scans of the 4935.03-Å atomic nitrogen line revealed its location upon a descending background toward lower wavelengths, possibly attributable to the R-branch tail of the $N_2^+(1-)(4,7)$ band. As a result, the line intensity was measured in the scanning mode to account for the background, which was determined at the line center by intersection with a line extended through the adjacent backgrounds. Slit widths of 250 μm provided a 2.7-Å spectral half-width. A scan was discarded if the beam current or pressure varied more than two percent. Figures 25 and 26 present quenching plots at 292 and 94 K, respectively, in which secondary quenching at both temperatures is seen. In Table 1, the value of $\tau = 4.27 \times 10^{-7}$ sec was calculated from atomic transition probabilities (Ref. 3). The observed quenching onset densities were much too large when compared with the calculated ones. Additional low density data would be needed to explain this discrepancy. Measured values of the second quenching constant are included in Table 2.

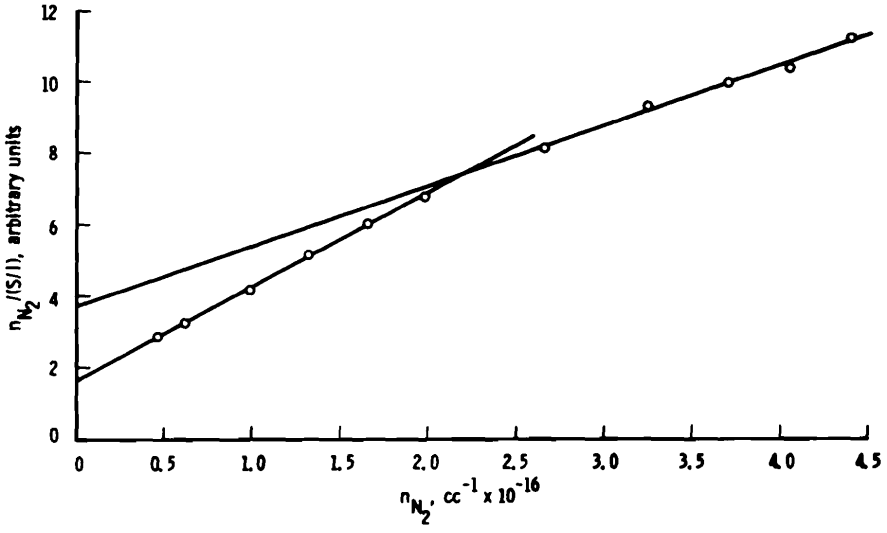

Figure 25. Quenching plot for $N[2p^2(^3P)4p\ ^2S^\circ_{1/2} \rightarrow 2p^2 3s\ ^2P_{3/2}]$ transition at 292 K.

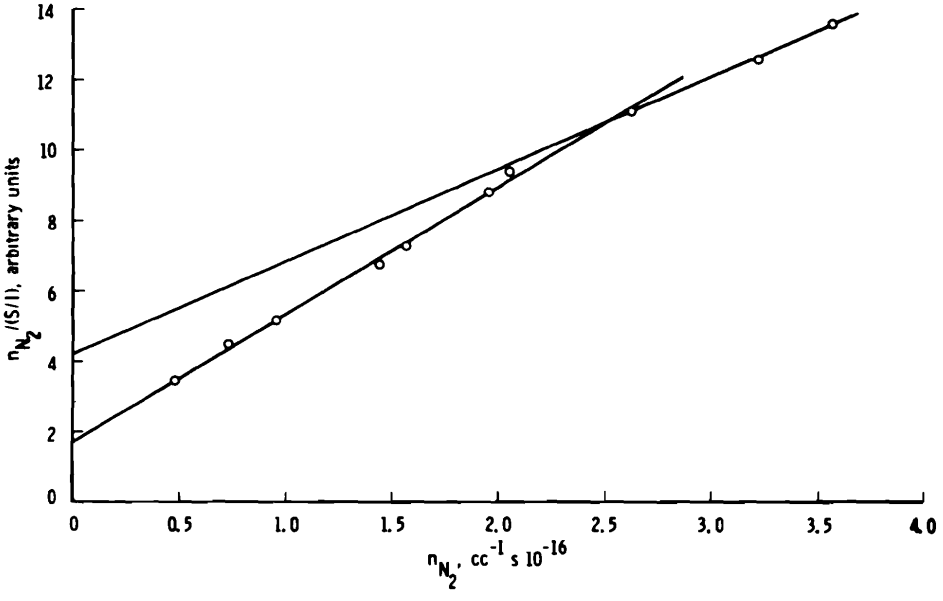

Figure 26. Quenching plot for $N[2p^2(^3P)4p\ ^2S^\circ_{1/2} \rightarrow 2p^2 3s\ ^2P_{3/2}]$ transition at 94 K.

3.7 $N^+ [2p(^2P^o)3d\ ^3F_4^o \rightarrow 2p3p\ ^3D_3]$

The transition $2s2p^2(^4P)3p\ ^5P_2^o \rightarrow 2s2p^2 3s\ ^5P_2$ also results in a line at 5005.14 Å, but its strength is expected to be only about three percent that of the $2p(^2P^o)3d\ ^3F_4^o$ $2p3p\ ^3D_3$ transition when reported line strengths are considered. A spectral scan of the immediate region showed the N^+ lines at 5001.15 and 5001.47 Å to appear as an unresolved pair of the approximate intensity of the 5001.14-Å line. Slit widths of 120 and 150 μm yielded halfwidths of 1.3 and 1.6 Å, respectively, sufficient for isolation and signal strength. The data were taken at fixed wavelength, but the weak background signals were determined from scans. Quenching plots for the two temperatures are shown in Figs. 27 and 28. From Ref. 3, the lifetime $\tau = 8.2 \times 10^{-9}$ sec was calculated.

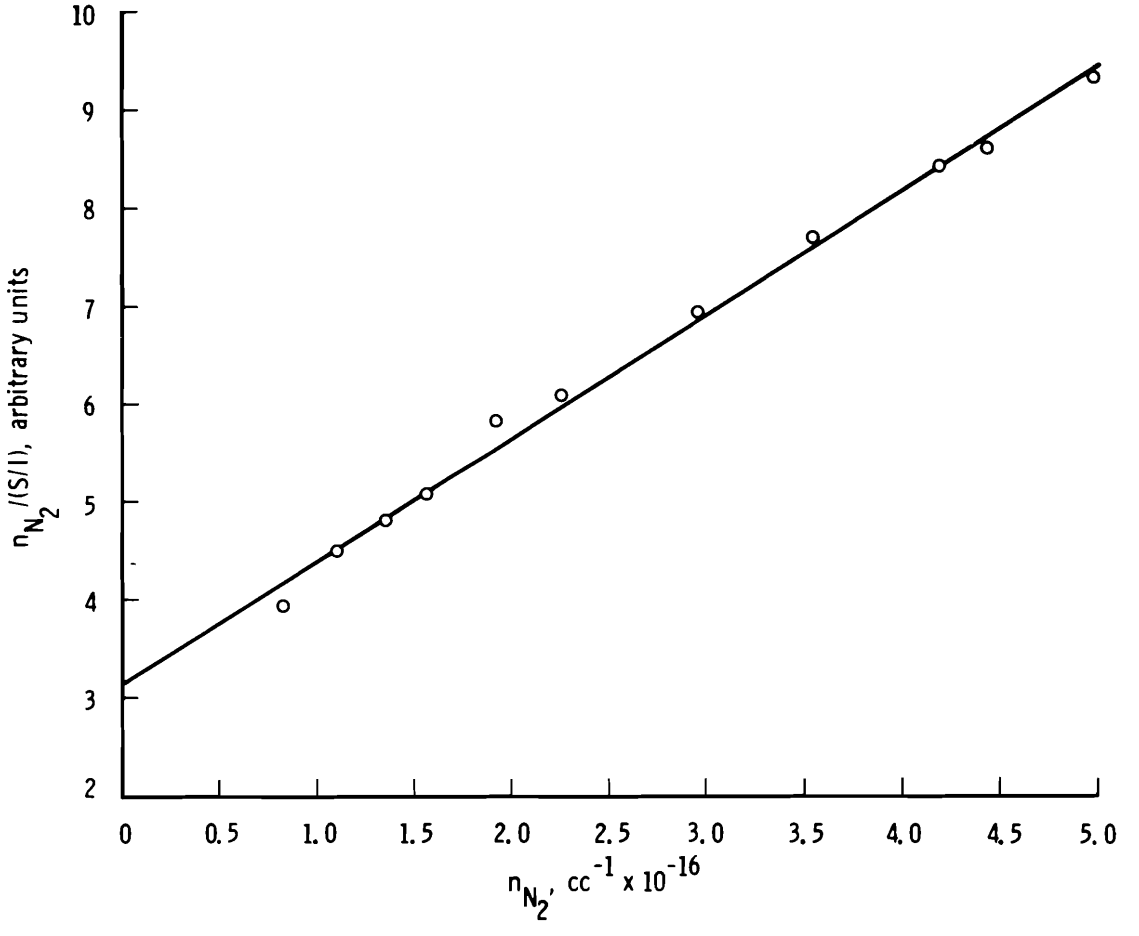

Figure 27. Quenching plot for $N^+ [2p(^2P^o)3d\ ^3F_4^o \rightarrow 2p3p\ ^3D_3]$ transition at 300 K.

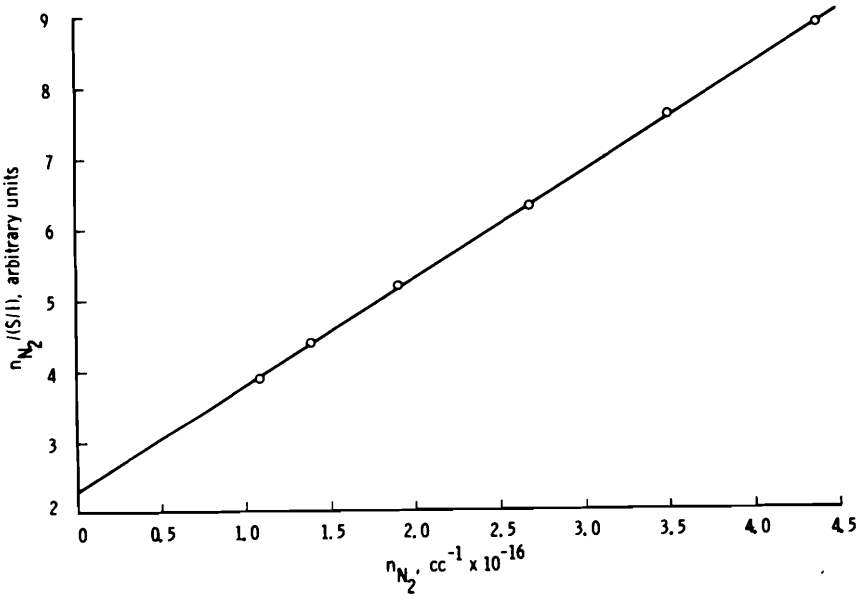

Figure 28. Quenching plot for $N^+ [2p(^2P^o)3d\ ^3F_4^o \rightarrow 2p3p\ ^3D_3]$ transition at 94 K.

4.0 DISCUSSION AND CONCLUSIONS

The quenching rate constants for various N_2^+, N^+, and N electronically excited energy levels were determined using the electron beam fluorescence technique. The variation of the results with N_2 density, beam current, and temperature was determined, and, additionally, resolved rotational line spectra of the $N_2^+(1-)(0,0)$ band were observed, yielding rate constants for the individual rotational levels. Distinct variations for k_i were found as T decreased from 300 to 94 K for all cases investigated, and the variation of k_i with rotational quantum number of the R branch of the $N_2^+(1-)(0,0)$ band was striking. It is planned that the results presented in this report will be analyzed, compared with existing energy transfer models, and discussed in more detail in a subsequent publication.

REFERENCES

1. Lewis, J. W. L. and Williams, W. D. "Collisional De-Excitation Cross-Section Measurement of Electronic States of Atomic and Molecular Hydrogen by Collision with Molecular Hydrogen." AEDC-TR-72-132 (AD750464), October 1972.

2. Bennett, R. G. and Dalby, F. W. "Experimental Determination of the Oscillator Strength of the First Negative Bands of N_2^+." The Journal of Chemical Physics, Vol. 31, No. 2, August 1959, pp. 434-441.

3. Wiese, W. L., Smith, M. W., and Miles, B. M. Atomic Transition Probabilities, Vol. 1. NSRDS-NB 4, U. S. Government Printing Office, Washington, D. C., 1966.

NOMENCLATURE

A_i	Einstein coefficient for level i
A_{ij}	Einstein coefficient for i-j transition
e	Electron and electronic charge
I	Beam current
k_e	Elastic rate constant
k_i	Quenching rate constant for level i
L	Electron beam length observed
M	Mach number
$\tilde{M}$	Reduced molecular weight of the collision partners
n_g	Gas number density of level g
P, P_∞	Pressure
Pr	Prandtl number
R	Universal gas constant
S	Radiative intensity
$S(\lambda)$	Wavelength dependent transmission factor
T	Static gas temperature
T_{max}	Centerline temperature
T_o	Wall temperature
T_R	Rotational temperature
α	Polarizability
γ	Specific heat ratio
λ	Wavelength
μ	Reduced mass
σ_i	Standard deviation
σ_{ij}	Excitation cross section for i to j transition
$\sigma^2_{in.}(i)$	Inelastic cross section for level i
τ_i	Radiative lifetime of level i
ω	Solid angle